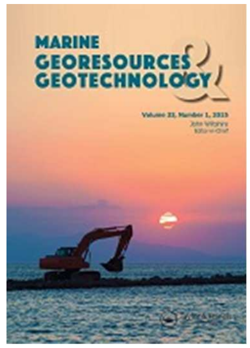

Deformation of a sandstone-mudstone particle mixture induced by periodic saturation

Journal:	*Marine Georesources & Geotechnology*
Manuscript ID	UMGT-2017-0087
Manuscript Type:	Original Article
Date Submitted by the Author:	18-Apr-2017
Complete List of Authors:	wang, jun-jie; School of River & Ocean Engineering, Chongqing Jiaotong University QIU, Zhen-Feng; National Engineering Research Center for Inland Waterway Regulation, Chongqing Jiaotong University Bai, Jiping; School of Engineering, Faculty of Computing, Engineering and Science, University of South Wales, Treforest Campus, United Kingdom, CF371DL Liu, Ming-Wei; School of River & Ocean Engineering, Chongqing Jiaotong University; National Inland Waterway Regulation Engineering Research Center,
Keywords:	deformation, periodic saturation, sandstone-mudstone particle mixture, axial strain, settlement

Table 1. Testing Scheme

Type of triaxial test	Confining pressure (kPa)	Number of periodic saturation (*N*)	Estimated stress level for periodic saturation (*L*)
Without periodic saturation	100, 200, 300, 400	/	/
With periodic saturation	100, 200, 300, 400	1, 5, 10, 20	0.25, 0.5, 0.75

Fig. 1. Curves of deviator stress against axial strain from triaxial tests without periodic saturation

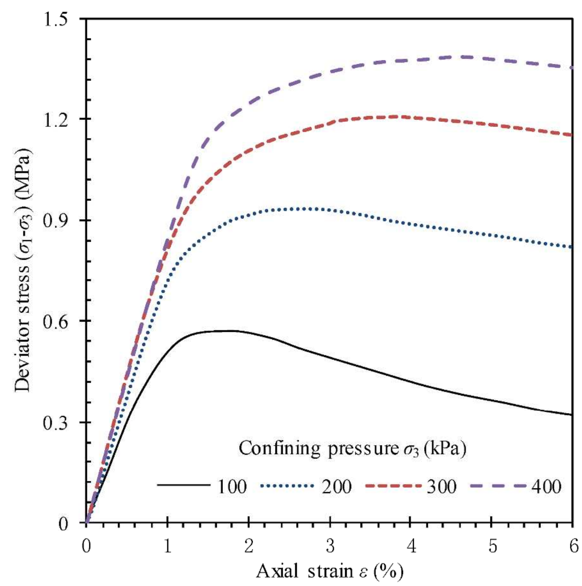

Fig. 1. Curves of deviator stress against axial strain from triaxial tests without periodic saturation

210x297mm (300 x 300 DPI)

Fig. 2. Typical curves of deviator stress against axial strain from triaxial tests with different numbers of periodic saturation at stress level about 0.5
(a) Confining pressure σ_3=100 kPa

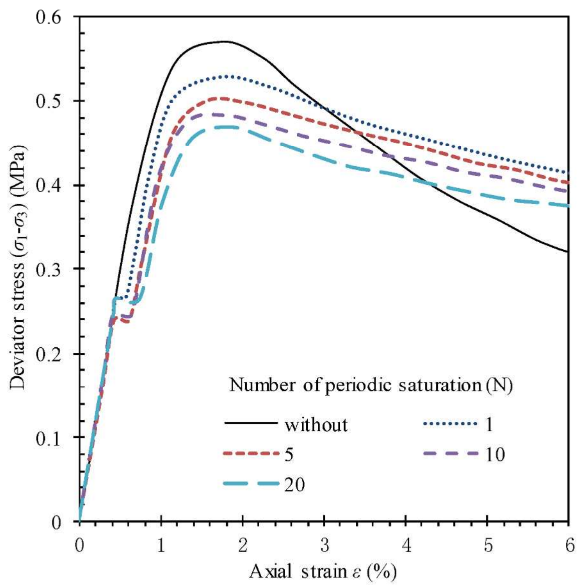

Fig. 2. Typical curves of deviator stress against axial strain from triaxial tests with different numbers of periodic saturation at stress level about 0.5
(a) Confining pressure σ3=100 kPa

210x297mm (300 x 300 DPI)

Fig. 2. Typical curves of deviator stress against axial strain from triaxial tests with different numbers of periodic saturation at stress level about 0.5

(b) Confining pressure σ_3=300 kPa

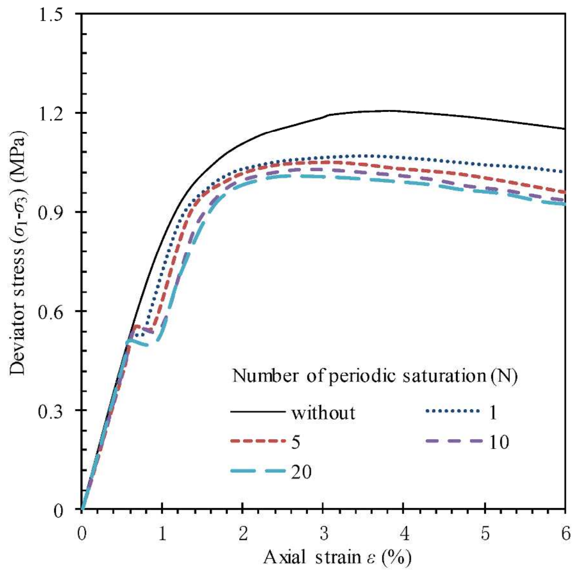

Fig. 2. Typical curves of deviator stress against axial strain from triaxial tests with different numbers of periodic saturation at stress level about 0.5
(b) Confining pressure σ3=300 kPa

210x297mm (300 x 300 DPI)

Fig. 3. Typical curves of deviator stress against axial strain from triaxial tests with periodic saturation for N=5 at different stress levels

(a) Confining pressure σ_3=100 kPa

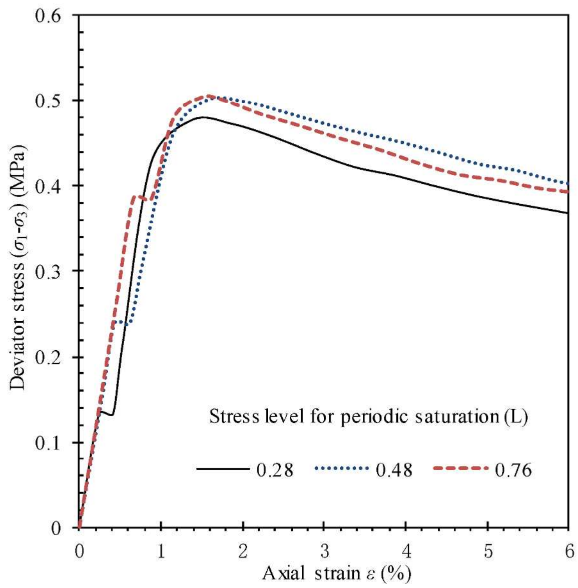

Fig. 3. Typical curves of deviator stress against axial strain from triaxial tests with periodic saturation for N=5 at different stress levels
(a) Confining pressure σ3=100 kPa

210x297mm (300 x 300 DPI)

Fig. 3. Typical curves of deviator stress against axial strain from triaxial tests with periodic saturation for N=5 at different stress levels

(b) Confining pressure σ_3=300 kPa

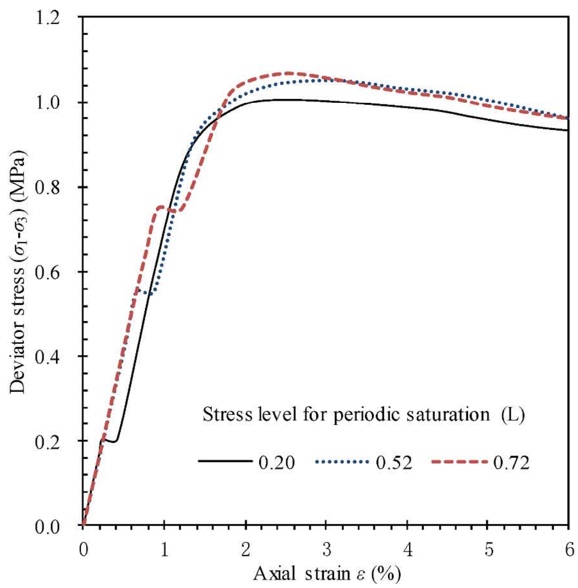

Fig. 3. Typical curves of deviator stress against axial strain from triaxial tests with periodic saturation for N=5 at different stress levels
(b) Confining pressure σ3=300 kPa

210x297mm (300 x 300 DPI)

Fig. 4. Definition of axial strain induced by periodic saturation ($\Delta\varepsilon$)

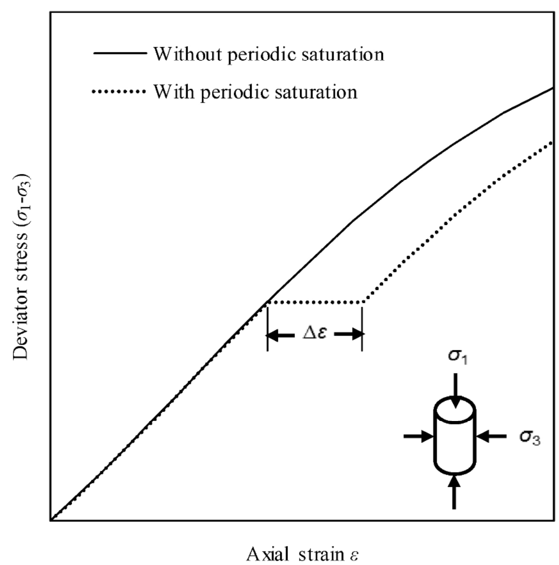

Fig. 4. Definition of axial strain induced by periodic saturation (Δε)

210x297mm (300 x 300 DPI)

Fig. 5. Effects of number of cycles on increment of axial strain induced by periodic saturation

(a) Confining pressure σ_3=100 kPa

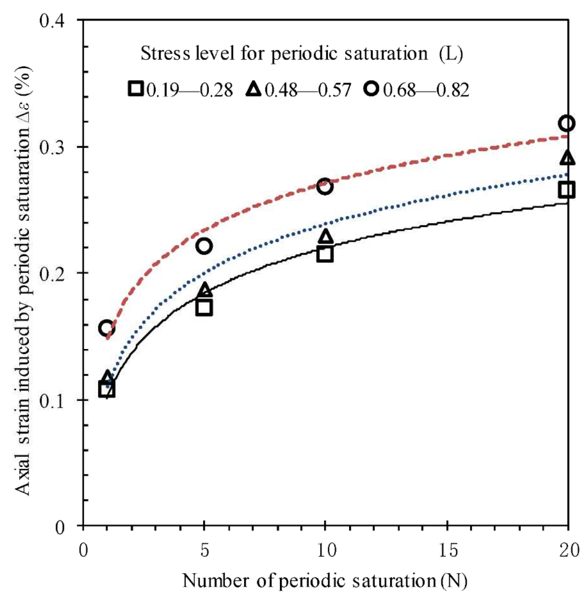

Fig. 5. Effects of number of cycles on increment of axial strain induced by periodic saturation
(a) Confining pressure σ3=100 kPa

210x297mm (300 x 300 DPI)

Fig. 5. Effects of number of cycles on increment of axial strain induced by periodic saturation

(b) Confining pressure σ_3=200 kPa

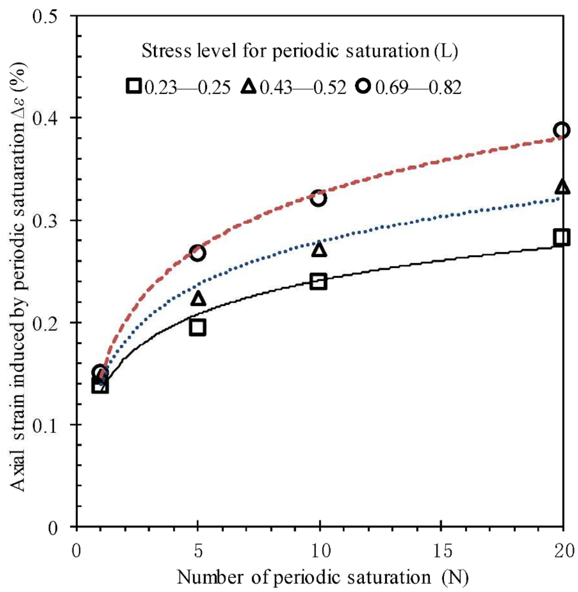

Fig. 5. Effects of number of cycles on increment of axial strain induced by periodic saturation (b) Confining pressure σ3=200 kPa

210x297mm (300 x 300 DPI)

Fig. 5. Effects of number of cycles on increment of axial strain induced by periodic saturation

(c) Confining pressure σ_3=300 kPa

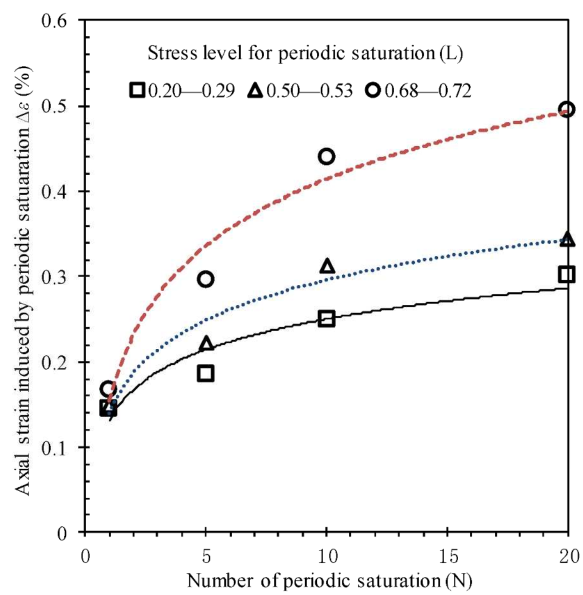

Fig. 5. Effects of number of cycles on increment of axial strain induced by periodic saturation
(c) Confining pressure σ3=300 kPa

210x297mm (300 x 300 DPI)

Fig. 5. Effects of number of cycles on increment of axial strain induced by periodic saturation

(d) Confining pressure σ_3=400 kPa

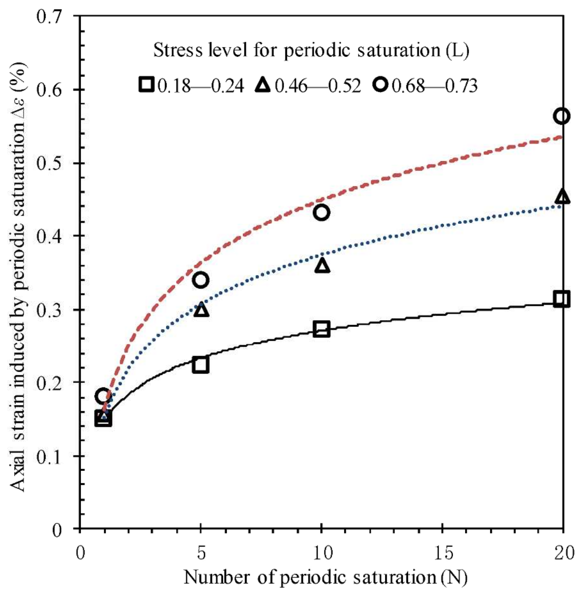

Fig. 5. Effects of number of cycles on increment of axial strain induced by periodic saturation
(d) Confining pressure σ3=400 kPa

210x297mm (300 x 300 DPI)

Fig. 6. Effects of stress level on increment of axial strain induced by periodic saturation

(a) Confining pressure σ_3=100 kPa

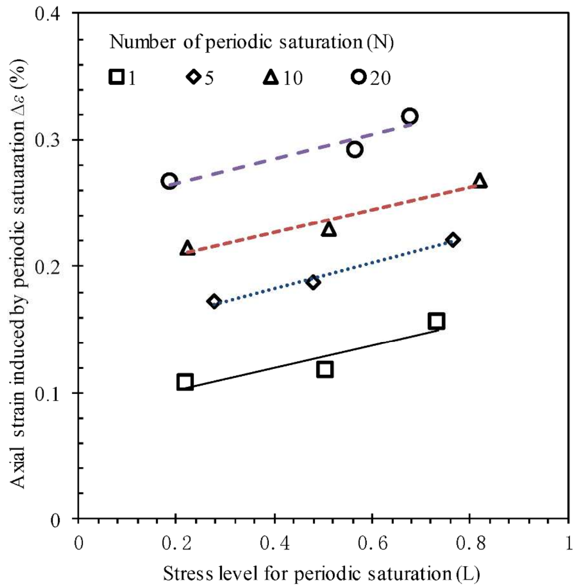

Fig. 6. Effects of stress level on increment of axial strain induced by periodic saturation
(a) Confining pressure σ3=100 kPa

210x297mm (300 x 300 DPI)

Fig. 6. Effects of stress level on increment of axial strain induced by periodic saturation

(b) Confining pressure σ_3=200 kPa

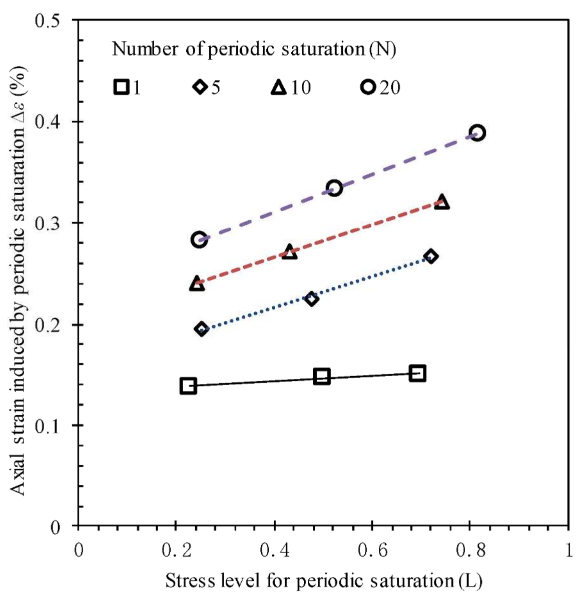

Fig. 6. Effects of stress level on increment of axial strain induced by periodic saturation
(b) Confining pressure σ3=200 kPa

210x297mm (300 x 300 DPI)

Fig. 6. Effects of stress level on increment of axial strain induced by periodic saturation

(c) Confining pressure σ_3=300 kPa

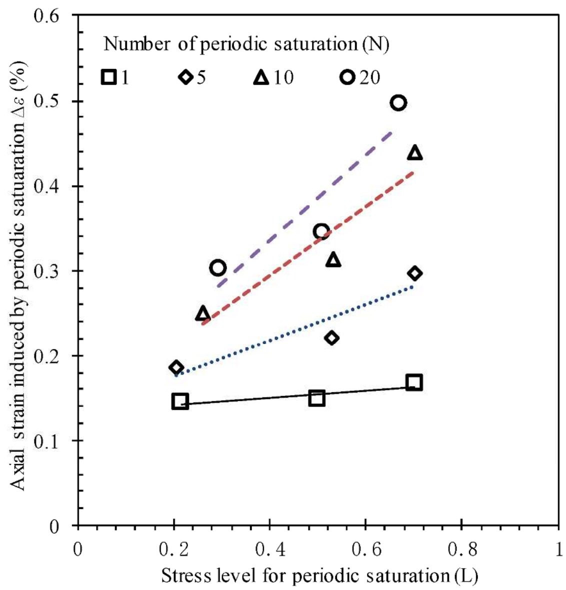

Fig. 6. Effects of stress level on increment of axial strain induced by periodic saturation
(c) Confining pressure σ3=300 kPa

210x297mm (300 x 300 DPI)

Fig. 6. Effects of stress level on increment of axial strain induced by periodic saturation

(d) Confining pressure σ_3=400 kPa

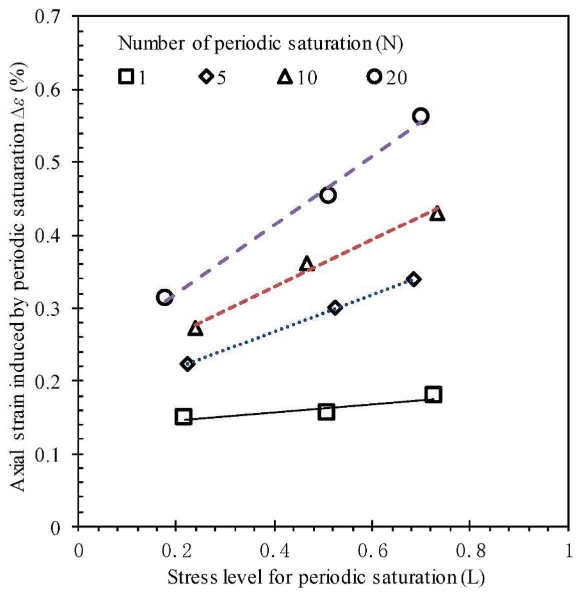

Fig. 6. Effects of stress level on increment of axial strain induced by periodic saturation
(d) Confining pressure σ3=400 kPa

210x297mm (300 x 300 DPI)

Fig. 7. Effects of confining pressure on increment of axial strain induced

by periodic saturation

(a) Stress level L=0.18 to 0.28 (mean 0.23)

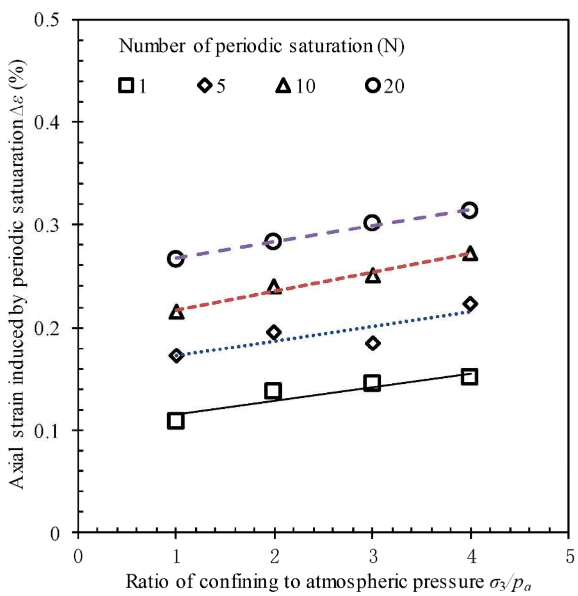

Fig. 7. Effects of confining pressure on increment of axial strain induced by periodic saturation
(a) Stress level L=0.18 to 0.28 (mean 0.23)

210x297mm (300 x 300 DPI)

Fig. 7. Effects of confining pressure on increment of axial strain induced

by periodic saturation

(b) Stress level L=0.43 to 0.57 (mean 0.50)

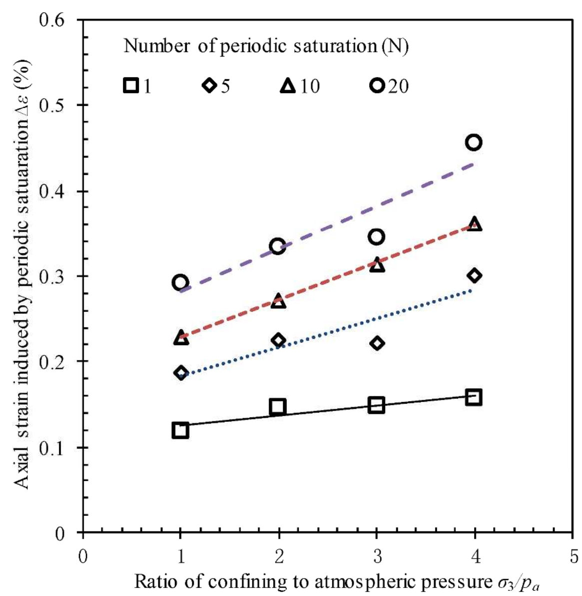

Fig. 7. Effects of confining pressure on increment of axial strain induced by periodic saturation
(b) Stress level L=0.43 to 0.57 (mean 0.50)

210x297mm (300 x 300 DPI)

Fig. 7. Effects of confining pressure on increment of axial strain induced by periodic saturation

(c) Stress level L=0.68 to 0.82 (mean 0.72)

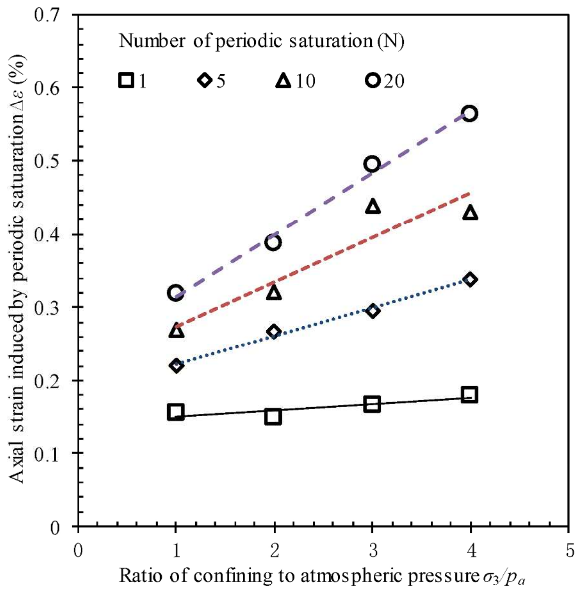

Fig. 7. Effects of confining pressure on increment of axial strain induced by periodic saturation (c) Stress level L=0.68 to 0.82 (mean 0.72)

210x297mm (300 x 300 DPI)

Fig. 8. A large-area foundation filled by sandstone-mudstone particle mixture subjected to periodic saturation

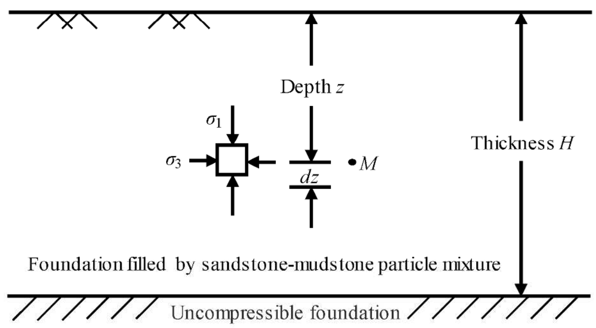

Fig. 8. A large-area foundation filled by sandstone-mudstone particle mixture subjected to periodic saturation

210x297mm (300 x 300 DPI)

Deformation of a sandstone-mudstone particle mixture induced by periodic saturation

Jun-Jie WANG [a]*, Zhen-Feng QIU [b], Jiping BAI [c], Ming-Wei LIU [d]

[a] Key Laboratory of Hydraulic and Waterway Engineering of Ministry of Education, Chongqing Jiaotong University, Chongqing 400074, P. R. China

[b] Engineering Research Center of Diagnosis Technology and Instruments of Hydro-Construction, Chongqing Jiaotong University, 66 Xuefu Road, Nan'an District, Chongqing 400074, PR China

[c] School of Engineering, Faculty of Computing, Engineering and Science, University of South Wales, Treforest Campus, United Kingdom, CF371DL

[d] National Engineering Research Center for Inland Waterway Regulation, Chongqing Jiaotong University, Chongqing 400074, P. R. China

* Corresponding Author.

E-mail address: wangjunjiehhu@163.com (J.-J. Wang)

429158988@qq.com (Z.-F. Qiu)

jiping.bai@southwales.ac.uk (J. Bai)

mingwei_liu@126.com (M.-W. Liu)

Abstract: This study focuses on the evaluation on deformation of a sandstone-mudstone particle mixture induced by periodic saturation. Two-type triaxial tests, without and with periodic saturation, were carried out. The strain-stress relationships from the two-type tests indicate that the periodic saturation may induce an increment of axial strain ($\Delta\varepsilon$), and the $\Delta\varepsilon$ values are related to the ratio of confining to atmospheric pressure (σ_3/p_a), stress level for periodic saturation (L) and number of periodic saturation or cycle (N). The values of $\Delta\varepsilon$ are increasing along logarithmic curves with increment of N value from 1 to 20, and increase along straight lines with increase L value from 0.18 to 0.82 or σ_3/p_a value from 1 to 4. Based on analyses of experimental data, a logarithmic fitting equation, which is a function of N, L and σ_3/p_a, was suggested to predict $\Delta\varepsilon$ value. And based on the fitting equation and simple analyses on stress state, another equation, which might be used to estimate the induced settlement by periodic saturation of a large-area foundation, was also suggested.

Key Words: deformation; periodic saturation; sandstone-mudstone particle mixture; axial strain; settlement

1. Introduction

Mixture of crushed sandstone and mudstone particles, as a common engineering fill in the Yangtze River Basin, especially in Chongqing, China, is widely used to construct earth-rock fill dams, slopes, highway embankments and airports, because of its good engineering characteristics (Wang et al. 2016a). The maximum thickness of filled foundation using the mixture has been greater than 150 m in several constructions of airports. And the maximum height of earth-rock fill dams constructed using the mixture as a main fill has also been higher than 100 m. The evaluation on post-construction settlement of the filled sandstone-mudstone particle mixture is very important. The settlement of the filled mixture is affected by many factors such as compaction effort (Wang et al. 2014b), particle size (Wang et al. 2015), content of mudstone particles (Wang et al. 2013; Wang et al. 2016b), and compression characteristics (Wang et al. 2016c).

While soils are filled in waterfront conditions, the water or wetting may affect the settlement because it affects the properties of the soils (Lim and Miller 2004; Park 2010; Thorel et al. 2011; Xu et al. 2007, 2011, 2016a and b) including the mixture of sandstone-mudstone particles (Wang et al. 2014a; Qiu and Wang 2015; Wang and Qiu 2017). While the mixture is filled along bank of or in a lager reservoir such as China's Yangtze River Three Gorges Project, it may be subjected to periodic saturation or cyclic wetting and drying induced by cyclic rising and lowering of reservoir water level. The Three Gorges Project is the largest hydroelectric project on record, with 1000 km^2 in area, 600 km in length, 2 km in width at the broadest section, 145 m in controlled level before flood, 175 m in normal water level, and 3.9×10^{10} m^3 in total storage. Its water level is therefore kept at between 145 m and 175 m, depending on flood control needs. The rising and lowering of water levels may affect the stability of slopes in waterfront conditions (Jia et al. 2009; Yan et al. 2010; Wang et al. 2012; Gao et al. 2013 and 2014). Periodic saturation induced by change of reservoir water level may also affect the post-construction settlement of the filled mixture. The investigation on the effects should be very interesting, although related works are scarcely reported.

It is worth mentioning that the periodic saturation conditions, induced by cyclic lowering and rising of reservoir water level, are different from the cyclic wetting and drying, induced by climatic conditions. Climatic conditions subject soils near the ground surface to cyclic drying and wetting, which may affect the behaviors of the soils (Rajaram and Erbach 1999; Guan et al. 2010; Ng and Leung 2012; Goh et al. 2014; Gallage and Uchimura 2016).

80 In this study, the effects of periodic saturation on deformation characteristics of the mixture were investigated by triaxial tests.

2. Test Material and Sample Preparation

An artificial mixture mixed by crushed sandstone and mudstone particles (PS and PM) with different diameters less than 20 mm was used as the test material in this study. Lightly weathered sandstone and mudstone blocks, excavated from a rocky mountain near the Yangtze River in Chongqing of China, were crushed to prepare the PS and PM. The uniaxial compressive strengths of the sandstone were tested, 60.0-72.2 MPa (natural state) and 60.0-67.4 MPa (saturated state), respectively. And ones of the mudstone are 17.6-25.8 MPa (natural state) and 8.3-15.0 MPa (saturated state). After crushing the sandstone and mudstone blocks, respectively, into particles smaller than 20 mm in diameter, the preparation of the test material includes three steps. The first step is to respectively sieve the PS and PM into different fractions with different sizes in accordance with Trade Standard of P. R. China SL237-006 (1999). The second step is to respectively mix the PS and PM according to the percentage in weight of eight different grain-size fractions as follows: 20-10 mm (18%), 10-5 mm (19%), 5-2 mm (19%), 2-1 mm (12%), 1-0.5 mm (10%), 0.5-0.25 mm (7%), 0.25-0.075 mm (12%), and <0.075 mm

(3%). And the last step is to mix the mixed PS and PM together according to ratio in weight 8:2 of PS to PM. The content by weight of PM of the test material is therefore about 20%. Based on the particle size distribution in the second step, the test material may be described as well-graded sand with gravel (SW) in accordance with the Unified Soil Classification System (USCS; ASTM 2000).

Cylindrical specimens with 101 mm in diameter and 200 mm in height were used in triaxial tests in this study. Each specimen was compacted in a trivalve split mold in five equal layers. The top surface of each layer was scarified before the compaction of the successive layer for better contact. The initial water content (w) and dry density (ρ_d) of each specimen are the same 8% and 1.92 g/cm^3, respectively.

3. Testing Scheme

In this study, two-type triaxial tests were carried out, in order to investigate the effects of periodic saturation on deformation of a crushed sandstone-mudstone particle mixture. One is common triaxial test without periodic saturation, and the other is the test with periodic saturation. In the two-type triaxial tests, the properties of each cylindrical specimen are the same, and they are 101 mm in diameter, 200 mm in height, 8% (or degree of saturation S=55%) in initial water content and 1.92 g/cm^3 in initial dry density. Four confining pressures, i.e. 100 kPa, 200kPa, 300 kPa and 400 kPa, are considered. The rate of vertical loading is 0.01 mm/min. And during the whole testing process, the specimen drains freely. For the triaxial test with periodic saturation, four different numbers of periodic saturation (*N*), i.e. 1, 5, 10 and 20, are selected, and three different stress levels (*L*) for periodic saturation, about 0.25, 0.50 and 0.75, are considered. The testing schemes are summarized in Table 1.

In this paper, the stress level (*L*) for periodic saturation is defined as the ratio of deviator stress (σ_1-σ_3), at which the specimen is subjected to periodic saturation, to crest of deviator stress $(\sigma_1\text{-}\sigma_3)_f$, where σ_1 and σ_3 are axial stress and confining pressure, respectively. Because the value of $(\sigma_1\text{-}\sigma_3)_f$ can only be determined according to tested strain-stress relationship curve, which can't be obtained until failure of specimen or finish of test, the value of *L* for periodic saturation can only be estimated firstly and is calculated after test according to experimental data.

4. Testing Procedure

The procedure of triaxial test with periodic saturation and one without periodic saturation are identical besides added "saturating" and "dewatering" steps in the former. After installation of specimen into triaxial cell, the specimen is applied confining pressure σ_3 from zero to one of 100 kPa, 200 kPa, 300 kPa and 400 kPa in 30 min, and the pressure is kept for 15 min. For the common triaxial test without periodic saturation, axial stress σ_1 is then applied with the rate of vertical loading 0.01 mm/min until failure of specimen or axial strain of 15%. But for the triaxial test with periodic saturation, axial stress σ_1 is applied to a scheduled value in 60 min, with the rate of vertical loading 0.01 mm/min and depending on estimated stress level for periodic saturation (*L*), and the stress state is kept for 30 min. Next, under the condition of keeping stress state, the specimen is saturated to degree of saturation (*S*) about 85% in 120 min by entering degassed water from its bottom, and this step is called as "saturating" step. After the saturating step, the specimen is dewatered to *S* about 55% (or *w* about initial 8%) in 120 min by entering hot air from its top, the stress state of specimen is still kept, and this step is called as "dewatering" step. Together steps "saturating" and "dewatering" is called one cycle of periodic saturation (Qiu 2016). For the tests with more than one cycle of periodic saturation, repeat of steps "saturating" and "dewatering" is necessary, under the condition of keeping the stress state of specimen. After periodic saturation, the specimen is sheared to failure or axial strain of 15% by applying axial stress σ_1 with the rate of vertical loading 0.01 mm/min.

5. Results and Analyses

5.1. Results

Figure 1 shows the strain-stress relationship curves of the crushed sandstone-mudstone particle mixture from the triaxial tests without periodic saturation. It is clear that the strain-stress relationship curves tend to soften, with an obvious peak point, and thus the crest of deviator stress, $(\sigma_1\text{-}\sigma_3)_f$, can easily be determined. It is also clear from the plots that the value of $(\sigma_1\text{-}\sigma_3)_f$ is increasing with increment of confining pressure, σ_3, and the value of axial strain (ε) corresponding to the $(\sigma_1\text{-}\sigma_3)_f$ is also increasing with increase σ_3.

Figure 2 shows the typical curves of deviator stress against axial strain from triaxial tests with different numbers of periodic saturation at estimated stress level about 0.5. For purpose of comparison conveniently, the strain-stress relationship curves from triaxial tests without periodic saturation are also given in the plots. It is clear from the plots that the strain-stress relationship curves of the test material are affected by the periodic saturation. And with increment of number of periodic saturation, *N*, the effects may be increasing.

Figure 3 shows the typical curves of strain-stress relationship of the test material from triaxial tests with periodic saturation for *N*=5 at different stress levels. It is clear that the selected stress level for periodic saturation

(L) may affect the strain-stress relationship.

Analyses of the experimental results shown in Figs. 2 and 3 indicate that the periodic saturation may affect the strain-stress relationship of the test material from two aspects. One is that periodic saturation may induce an increment of axial strain under the conditions of keeping the stress state of specimen constant. The other is that the value of crest of deviator stress obtained from the curve of deviator stress against axial strain is reduced by periodic saturation. Owing to space constraints, this paper investigated only the increment of axial strain ($\Delta\varepsilon$) induced by periodic saturation (Fig.4). The value of $\Delta\varepsilon$ may affected by the confining pressure (σ_3), stress level for periodic saturation (L) and number of periodic saturation or cycle (N).

5.2. Effects of N on $\Delta\varepsilon$

Figure 5 shows the variation of increment of axial strain induced by periodic saturation ($\Delta\varepsilon$) (defined in Fig.4) with the number of periodic saturation (N) for different confining pressures (σ_3). It is clear from the plots that, for any of four values of σ_3 100 kPa, 200 kPa, 300 kPa and 400 kPa, the values of $\Delta\varepsilon$ are increasing along logarithmic curves with increment of N value from 1 to 20. The relationship between the values of $\Delta\varepsilon$ and N may be expressed by a logarithmic function as follows:

$$\Delta\varepsilon = A_1 \ln N + B_1 \quad (1)$$

where $\Delta\varepsilon$ is the increment of axial strain induced by periodic saturation (%); N is the number of periodic saturation, and N=1, 2, 3,⋯, 20; A_1 and B_1 are two coefficients, which may be determined by fitting test data shown in Fig.5 using Eq.(1).

From Fig.5a for the case with the confining pressure σ_3=100 kPa, it is clear that, while increasing N value from 1 to 20, the $\Delta\varepsilon$ values are increasing from 0.11% to 0.27% for L=0.19-0.28, 0.12% to 0.29% for L=0.48-0.57 and 0.16% to 0.32% for L=0.68-0.82. From Fig.5b for the case with σ_3=200 kPa, the $\Delta\varepsilon$ values are increasing from 0.14% to 0.28% for L=0.23-0.25, 0.15% to 0.33% for L=0.43-0.52 and 0.15% to 0.39% for L=0.69-0.82. From Fig.5c for the case with σ_3=300 kPa, the $\Delta\varepsilon$ values are increasing from 0.15% to 0.30% for L=0.20-0.29, 0.15% to 0.34% for L=0.50-0.53 and 0.17% to 0.50% for L=0.68-0.72. And from Fig.5d for the case with σ_3=400 kPa, the $\Delta\varepsilon$ values are increasing from 0.15% to 0.31% for L=0.18-0.24, 0.16% to 0.45% for L=0.46-0.52 and 0.18% to 0.56% for L=0.68-0.73.

5.3. Effects of L on $\Delta\varepsilon$

Figure 6 shows the effects of stress level for periodic saturation (L) on the

220 increment of axial strain induced by periodic saturation ($\Delta\varepsilon$) for four
221 cases with the confining pressures σ_3=100 kPa, 200 kPa, 300 kPa and 400
222 kPa, respectively. It is clear from the plots that the values of $\Delta\varepsilon$ are
223 increasing along straight lines with increment of L value. The relationship
224 between the values of $\Delta\varepsilon$ and L may be expressed by:

225 $$\Delta\varepsilon = A_2 L + B_2 \quad (2)$$

226 where L is the stress level for periodic saturation, and L=0 to 1; A_2 and B_2
227 are two coefficients, which may be determined by fitting test data shown
228 in Fig.6 using Eq.(2).

229 It is clear from Fig.6a for the case with the confining pressure σ_3=100 kPa
230 that, with increasing L value from 0.19 to 0.82, the $\Delta\varepsilon$ values are
231 increasing from 0.11% to 0.16% for N=1, 0.17% to 0.22% for N=5,
232 0.22% to 0.27% for N=10 and 0.27% to 0.32% for N=20. From Fig.6b for
233 the case with σ_3=200 kPa, with increasing L value from 0.23 to 0.82, the
234 $\Delta\varepsilon$ values are increasing from 0.14% to 0.15% for N=1, 0.20% to 0.27%
235 for N=5, 0.24% to 0.32% for N=10 and 0.28% to 0.39% for N=20. From
236 Fig.6c for the case with σ_3=300 kPa, with increasing L value from 0.20 to
237 0.72, the $\Delta\varepsilon$ values are increasing from 0.14% to 0.17% for N=1, 0.19%
238 to 0.30% for N=5, 0.25% to 0.44% for N=10 and 0.30% to 0.50% for
239 N=20. And from Fig.6d for the case with σ_3=400 kPa, with increasing L

value from 0.18 to 0.73, the $\Delta\varepsilon$ values are increasing from 0.15% to 0.18% for N=1, 0.22% to 0.34% for N=5, 0.27% to 0.43% for N=10 and 0.31% to 0.56% for N=20.

5.4. Effects of σ_3 on $\Delta\varepsilon$

In order to display the effects of the confining pressure (σ_3) on the increment of axial strain ($\Delta\varepsilon$) induced by periodic saturation, Figure 7 shows the variation of $\Delta\varepsilon$ values with the ratio of confining to atmospheric pressure (σ_3/p_a), where the p_a value equals to 100 kPa. It is clear from the plots that the values of $\Delta\varepsilon$ are increasing along straight lines with increment of ratio σ_3/p_a value. The relationship between the values of $\Delta\varepsilon$ and σ_3/p_a may be expressed by:

$$\Delta\varepsilon = A_3\frac{\sigma_3}{p_a} + B_3 \qquad (3)$$

where σ_3/p_a is the ratio of confining to atmospheric pressure, and p_a=100 kPa and σ_3/p_a=1 to 4; A_3 and B_3 are two coefficients, which may be determined by fitting test data shown in Fig.7 using Eq.(3).

It is clear from Fig.7a for the case with the stress level for periodic saturation L=0.18 to 0.28 (mean 0.23) that, with increasing σ_3/p_a value from 1 to 4, the $\Delta\varepsilon$ values are increasing from 0.11% to 0.15% for N=1, 0.17% to 0.22% for N=5, 0.22% to 0.27% for N=10 and 0.27% to 0.31% for N=20. From Fig.7b for the case with the stress level L=0.43 to 0.57 (mean 0.50), with increasing σ_3/p_a value from 1 to 4, the $\Delta\varepsilon$ values are increasing from 0.12% to 0.16% for N=1, 0.19% to 0.30% for N=5, 0.23% to 0.36% for N=10 and 0.29% to 0.45% for N=20. And from Fig.7c for the case with L=0.68 to 0.82 (mean 0.72), with increasing σ_3/p_a value from 1 to 4, the $\Delta\varepsilon$ values are increasing from 0.15% to 0.18% for N=1, 0.22% to 0.34% for N=5, 0.27% to 0.43% for N=10 and 0.32% to 0.56% for N=20.

5.5. An equation to predict $\Delta\varepsilon$

The variation of $\Delta\varepsilon$ value with increment of N value may be expressed by a logarithmic function as shown in Eq.(1), one with increment of L value expressed by a linear function as shown in Eq.(2), and one with increasing σ_3/p_a value also expressed by a linear function as shown in Eq.(3), thus the value of $\Delta\varepsilon$, which is dependent on N, L and σ_3/p_a values, may be predicted by a logarithmic function as follows:

$$\Delta\varepsilon=\left[\left(a_1\frac{\sigma_3}{p_a}+b_1\right)L+\left(c_1\frac{\sigma_3}{p_a}+d_1\right)\right]\ln N+\left[\left(a_2\frac{\sigma_3}{p_a}+b_2\right)L+\left(c_2\frac{\sigma_3}{p_a}+d_2\right)\right] \quad (4)$$

where $\Delta\varepsilon$ is the increment of axial strain induced by periodic saturation

(%); N is the number of periodic saturation, and N=1, 2, 3,⋯, 20; L is the stress level for period saturation, and L=0 to 1; σ_3/p_a is the ratio of confining to atmospheric pressure, and p_a=100 kPa and σ_3/p_a=1 to 4; a_1, b_1, c_1, d_1, a_2, b_2, c_2 and d_2 are eight coefficients, which may be determined by fitting test data shown in Figs.5, 6 and 7 using Eq.(4).

Based on determined values of the eight coefficients a_1, b_1, c_1, d_1, a_2, b_2, c_2 and d_2, Eq.(4) can be rewritten as follows:

$$\Delta\varepsilon=\left[\left(0.048\frac{\sigma_3}{p_a}-0.036\right)L+\left(-0.010\frac{\sigma_3}{p_a}+0.056\right)\right]\ln N+\left[\left(-0.016\frac{\sigma_3}{p_a}+0.091\right)L+\left(0.018\frac{\sigma_3}{p_a}+0.069\right)\right] \quad (4a)$$

6. Settlement induced by periodic saturation

Periodic saturation may increase settlement of filled foundation because it may induce an increment of axial strain ($\Delta\varepsilon$). Evaluation on the settlement induced by periodic saturation is very important for the foundation filled in or along bank of a large reservoir such as China's Yangtze River Three Gorges Reservoir. In order to estimate the settlement induced by periodic saturation of a foundation filled by sandstone-mudstone particle mixture, a computational example is analyzed in this section.

Description of computational example (Fig.8): a large-area foundation filled by crushed sandstone-mudstone particle mixture on a horizontal uncompressible foundation, with *H* in thickness, is subjected to periodic saturation.

In order to estimate the stress state at any point (*M*) with a depth *z* in the filled foundation (Fig.8), assuming that the filled mixture is under normal consolidation conditions and the coefficient of earth pressure at rest (K_0) of the mixture can be estimated by (Jâky 1948):

$$K_0 = 1 - \sin\varphi \qquad (5)$$

where K_0 is the coefficient of earth pressure at rest; And φ is the angle of shearing resistance (deg), which is defined as the dip angle of a straight line tangent to Mohr's stress circle and through the origin, in the plot of shear stress against normal stress. The angle φ is also determined by the equation as follows:

$$\varphi = \sin^{-1}\frac{(\sigma_1 - \sigma_3)_f}{(\sigma_1 + \sigma_3)_f} \qquad (6)$$

Based on Eq.(5), the stress state at the point *M* with the depth *z* in the foundation (Fig.8) is given by:

$$\left.\begin{array}{l}\sigma_1 = \gamma z \\ \sigma_3 = (1-\sin\varphi)\sigma_1\end{array}\right\} \quad (7)$$

where γ is the unit weight of the filled foundation (kN/m^3); And z is the depth of the point M in the foundation (m).

Based on Eqs.(6) and (7) and the definition of stress level (L), the value of L at the point M with the depth z in the foundation (Fig.8) is given by:

$$L = \frac{\sigma_1 - \sigma_3}{(\sigma_1 - \sigma_3)_f} = 0.5 \quad (8)$$

Substitute L=0.5 into Eq.(4a), and consider the definition of axial strain, the derivative of settlement induced by periodic saturation (dS_p) for the derivative of depth z (dz) may be calculated by:

$$dS_p = \frac{1}{100}\left[\left(\frac{0.014(1-\sin\varphi)\gamma z}{p_a} + 0.038\right)\ln N + \left(\frac{0.010(1-\sin\varphi)\gamma z}{p_a} + 0.115\right)\right]dz \quad (9)$$

where dS_p is the derivative of settlement induced by periodic saturation; And dz is the derivative of depth z.

The settlement induced by periodic saturation (S_p) can be obtained by integrating the right of Eq.(9) from zero to H, and is given by:

$$
\begin{aligned}
S_p &= \int_0^H \frac{1}{100}\left\{\left[\frac{\gamma\left(1-\sin\varphi\right)\left(0.014\ln N+0.010\right)}{p_a}\right]z+\left(0.038\ln N+0.115\right)\right\}dz \\
&= \frac{\gamma\left(1-\sin\varphi\right)\left(0.007\ln N+0.005\right)}{100\,p_a}H^2+\frac{0.038\ln N+0.115}{100}H
\end{aligned}
\qquad (10)
$$

where S_p is the settlement induced by periodic saturation (m); H is the thickness of filled foundation subjected to periodic saturation (m); γ is the unit weight of the filled foundation (kN/m^3); φ is the angle of shearing resistance (deg); p_a is the atmospheric pressure (kPa), and p_a=100 kPa; And N is the number of periodic saturation, and N=1, 2, 3,⋯, 20.

7. Conclusions

While a foundation, which was filled by a sandstone-mudstone particle mixture, is in of along bank of a large reservoir, it may be subjected to periodic saturation induced by cyclic rising and lowering of reservoir water level. Periodic saturation may induce settlement of the foundation because it may induce deformation of the mixture. In order to investigate the deformation of the sandstone-mudstone particle mixture induced by periodic saturation, two-type triaxial tests were carried out. One is common triaxial test without periodic saturation, and the other is triaxial test with periodic saturation. Comparison of the strain-stress relationship curves from the two-type triaxial tests indicates that an increment of axial strain ($\Delta\varepsilon$) may be induced by periodic saturation. The value of $\Delta\varepsilon$ may affected by the confining pressure (σ_3), stress level for periodic saturation (L) and number of periodic saturation or cycle (N). Based on analyses of experimental data, the following conclusions can be drawn:

(1) While only increasing N value from 1 to 20, the values of $\Delta\varepsilon$ are increasing along logarithmic curves. The minimum value of $\Delta\varepsilon$ is about 0.11% for the case with N=1, L=0.19 and σ_3=100 kPa, and the maximum value about 0.56% for the case with N=20, L=0.73 and σ_3=400 kPa,

(2) Under the conditions of the same N value, the values of $\Delta\varepsilon$ are increasing along straight lines with increment of stress level (L) or ratio of confining to atmospheric pressure (σ_3/p_a) values.

(3) Variation of $\Delta\varepsilon$ value with parameters N, L and σ_3/p_a may be predicted by a logarithmic fitting equation.

(4) Based on the fitting equation of $\Delta\varepsilon$ and simple analyses on stress state in a large-area foundation, which was filled by sandstone-mudstone particle mixture on a horizontal uncompressible foundation and in normal consolidation conditions, the settlement induced by periodic saturation may be predicted easily.

Acknowledgements

The authors gratefully acknowledge financial support from the National Natural Science Foundation of China under Grant No. 51479012 and 51479014, the National Science and Technology Support Program of China under Grant No. 2015BAK09B01, and the Chongqing Science and Technology Commission of China under Grant No. cstc2015jcyjBX0139, respectively.

References

ASTM. (2000). Standard practice for classification of soils for engineering purposes (Unified Soil Classification System). D2487, West Conshohocken, PA.

Gallage, C., Uchimura, T. (2016). Direct shear testing on unsaturated silty soils to investigate the effects of drying and wetting on shear strength parameters at low suction. Journal of Geotechnical and Geoenvironmental Engineering, ASCE 142(3), 04015081.

Gao, Y.F., Zhang, F., Lei, G.H., Li, D.Y. (2013). An extended limit analysis of three-dimensional slope stability. Géotechnique 63(6), 518-524.

Gao, Y.F., Zhu, D.S., Zhang, F., Lei, G.H., Qin, H.Y. (2014). Stability analysis of three-dimensional slopes under water drawdown conditions. Canadian Geotechnical Journal 51(11), 1355-1364.

Goh, S.G., Rahardjo, H., Leong, E.C. (2014). Shear strength of unsaturated soils under multiple drying-wetting cycles. Journal of Geotechnical and Geoenvironmental Engineering, ASCE 140(2), 06013001.

Guan, G.S., Rahardjo, H., Choon L.E. (2010). Shear strength equations for unsaturated soil under drying and wetting. Journal of Geotechnical and Geoenvironmental Engineering, ASCE 136(4), 594–606.

Jâky, J. (1948). Pressure in soils. Proceedings of the 2nd International Conference on Soil Mechanics and Foundation Engineering 1, 103-107.

Jia, G.W., Zhan, T.L.T., Chen, Y.M. Fredlund, D.G. (2009). Performance of a large-scale slope model subjected to rising and lowering water levels. Engineering Geology 106, 92–103.

Lim, Y., Miller, G. (2004). Wetting-induced compression of compacted Oklahoma soils. Journal of Geotechnical and Geoenvironmental Engineering, ASCE 130(10), 1014-1023.

Ng, C.W.W., Leung, A.K. (2012). Measurements of drying and wetting permeability functions using a new stress-controllable soil column. Journal of Geotechnical and Geoenvironmental Engineering, ASCE 138(1), 58-68.

Park, S. (2010). Effect of wetting on unconfined compressive strength of cemented sands. Journal of Geotechnical and Geoenvironmental Engineering, ASCE 136(12), 1713–1720.

Qiu, Z.-F. (2016). Triaxial deformation behavior and damage model under wet-dry cycling of a sandstone-mudstone mixture. Ph.D. dissertation, Chongqing Jiaotong University, P.R. China.

Qiu, Z.-F., Wang, J.-J. (2015). Experimental study on the anisotropic hydraulic conductivity of a sandstone-mudstone particle mixture. Journal of Hydrologic Engineering, ASCE 20(11), 04015029.

Rajaram, G., Erbach, D.C. (1999). Effect of wetting and drying on soil physical properties. Journal of Terramechanics 36(1), 39-49.

Thorel, L., Ferber, V., Caicedo, B., Khokhar, I.M. (2011). Physical modelling of wetting-induced collapse in embankment base. Géotechnique 61(5), 409–420.

Trade Standard of P. R. China, SL237-006. (1999). Standard method for particle size distribution of soils. In Specification of Soil Test, The Ministry of Water Resources of P. R. China, Beijing, P. R. China (in Chinese).

Wang, J.-J., Cheng, Y.-Z., Zhang, H.-P., Deng, D.-P. (2015). Effects of particle size on compaction behavior and particle crushing of crushed sandstone-mudstone particle mixture. Environmental Earth Sciences 73(12), 8053-8059.

Wang, J.-J., Fang, X.-S., Qiu, Z.-F. (2016a). Engineering properties of a sandstone-mudstone particle mixture. Science Press, P.R. China (in Chinese)

Wang, J.-J., Qiu, Z.-F. (2017). Anisotropic hydraulic conductivity and critical hydraulic gradient of a crushed sandstone–mudstone particle mixture. Marine Georesources & Geotechnology 35(1), 89-97.

Wang, J.-J., Qiu, Z.-F., Deng, W.-J. (2014a) Shear strength of a crushed sandstone-mudstone particle mixture. International Journal of Architectural Engineering Technology 1, 33-37.

Wang, J.-J., Qiu, Z.-F., Deng, W.-J., Zhang, H.-P. (2016b). Effects of mudstone particle content on shear strength of a crushed sandstone-mudstone particle mixture. Marine Georesources &

Geotechnology 34(4), 395-402.

Wang, J.-J., Qiu, Z.-F., Hao, J.-Y., Zhang, J.-T. (2016c). Compression characteristics of an artificially mixed soil from confined uniaxial compression tests. Environmental Earth Sciences 75, 152.

Wang, J.-J., Zhang, H.-P., Deng, D.-P. (2014b). Effects of compaction effort on compaction behavior and particle crushing of a crushed sandstone-mudstone particle mixture. Soil Mechanics and Foundation Engineering 51(2), 67-71.

Wang, J.-J., Zhang, H.-P., Deng, D.-P., Liu, M.-W. (2013). Effects of mudstone particle content on compaction behavior and particle crushing of a crushed sandstone－mudstone particle mixture. Engineering Geology 167, 1-5.

Wang, J.-J., Zhang, H.-P., Zhang, L., and Liang, Y. (2012). Experimental study on heterogeneous slope responses to drawdown. Engineering Geology 147-148, 52–56.

Xu, W.-J., Hu, R.-L., Tan, R.J. (2007). Some geomechanical properties of soil-rock mixtures in the Hutiao gorge area, China. Géotechnique, 57(3): 255-264.

Xu, W.-J., Hu, L.-M., Gao, W. (2016a). Random generation of the meso-structure of a soil-rock mixture and its application in the study of the mechanical behavior in a landslide dam. International Journal of Rock Mechanics & Mining Sciences 86: 166–178.

Xu, W.-J., Wang, S., Zhang, H.-Y., Zhang, Z.-L. (2016b). Discrete element modelling of a soil-rock mixture used in an embankment dam. International Journal of Rock Mechanics & Mining Sciences 86: 141–156.

Xu, W.-J., Xu, Q., Hu, R.-L. (2011). Study on the shear strength of soil–rock mixture by large scale direct shear test. International Journal of Rock Mechanics and Mining Sciences 48(8):1235 -1247.

Yan, Z.-L., Wang, J.-J, Chai, H.-J. (2010). Influence of water level fluctuation on phreatic line in silty soil model slope. Engineering Geology 113(1-4), 90-98.